Negative Thermal Expansion, Response to Pressure and Phase Transitions in $CaTiF_6$

Brett R. Hester,[†] and Angus P. Wilkinson*[,†,§]

[†] School of Chemistry and Biochemistry, Georgia Institute of Technology, Atlanta, GA 30332-0400, United States

[§]School of Materials Science and Engineering, Georgia Institute of Technology, Atlanta, GA 30332-0245, United States

ABSTRACT: Strong volume negative thermal expansion over a wide temperature range typically only occurs in ReO_3-type fluorides that retain an ideal cubic structure to very low temperatures, such as ScF_3, $CaZrF_6$, $CaHfF_6$ and $CaNbF_6$. $CaTiF_6$ was examined in an effort to expand this small family of materials. However, it undergoes a cubic ($Fm\bar{3}m$) to rhombohedral ($R\bar{3}$) transition on cooling to ~120 K, with a minimum volume coefficient of thermal expansion (CTE) close to -42 ppm K^{-1} at 180 K and a CTE of about -32 ppm K^{-1} at room temperature. On compression at ambient temperature, the material remains cubic to ~0.25 GPa with $K_0 = 29(1)$ GPa and $K'_0 = -50(5)$. Cubic $CaTiF_6$ is elastically softer, and shows more pronounced pressure induced softening, than both $CaZrF_6$ and $CaNbF_6$. In sharp contrast to both $CaZrF_6$ and $CaNbF_6$, $CaTiF_6$ undergoes a first order pressure induced octahedral tilting transition to a rhombohedral phase ($R\bar{3}$) on compression above 0.25 GPa, which is closely related to that seen in ScF_3. Just above the transition pressure, this phase is elastically very soft with a bulk modulus of only ~4 GPa as octahedral tilting associated with a reduction in the Ca-F-Ti angles provides a low energy pathway for volume reduction. This volume reduction mechanism leads to highly anisotropic elastic properties, with the rhombohedral phase displaying both a low bulk modulus and negative linear compressibility parallel to the crystallographic c-axis for pressures below ~ 2.5 GPa. At ~3 GPa a further phase transition to a poorly ordered phase occurs.

1. INTRODUCTION

Control of thermal expansion is highly desirable for applications where dimensional stability or good thermal shock resistance are needed. The fabrication of composites from mixtures of positive and negative thermal expansion (NTE) materials[1-8] is a possible route for creating tailored thermal expansion materials.[9] However, in such composites the expansion mismatch between different components induces stresses on the materials, which can adversely affect their expansion characteristics.[2, 5, 10-12] Therefore, the response of NTE materials to stress, or less generally pressure, needs to be understood along with their expansion characteristics.

Several distinct mechanisms for NTE are well established.[13-14] In materials where phase transitions of various types are involved, strong NTE may occur over a somewhat limited temperature range, for example, $Bi_{0.95}La_{0.05}NiO_3$ (α_L= -82 ppm/K, ΔT: 320-380 K), $SrCu_3Fe_4O_{12}$ (α_L= -22.6 ppm/K, ΔT: 200-230 K), $(Mn_{0.96}Fe_{0.04})_3(Zn_{0.5}Ge_{0.5})N$ (α_L= -25 ppm/K, ΔT: 316-386 K), and $MnCo_{0.98}Cr_{0.02}Ge$ (α_L= -116 ppm/K, ΔT: 250-305 K .[15-18]

In open framework solids, with a phonon mechanism for negative thermal expansion, NTE can be present over a very wide temperature range, for example ZrW_2O_8 (α_L= -8.7 ppm/K, ΔT: 0.3-693 K), ScF_3 (α_L= -5 ppm/K, ΔT: 10 - 1000 K), $[Cu_3(btc)_2]$ (α_L= -4.1 ppm/K, ΔT: 80-500 K), and $Zn(CN)_2$ (α_L= -16.9 ppm/K, ΔT: 25-375 K).[19-22] However, open framework NTE materials frequently undergo structural phase transition on modest compression, which can make their application in composites problematic.[23-24]

Amongst open framework NTE materials, there has been considerable recent interest in metal fluorides with ReO_3-related structures.[22, 25-38] Using an appropriate choice of metal cations, low or negative thermal expansion can be combined with optical transparency ranging from the mid-IR into the UV, which is potentially valuable for multispectral optical applications.[28] Strong negative thermal expansion in ReO_3-type fluorides is typically found in compositions that maintain an ideal cubic structure to very low temperatures, for example, ScF_3,[22] $CaHfF_6$, $CaZrF_6$[28] and $CaNbF_6$.[26] However, only a small subset of ReO_3-type fluorides, where the cations are very electropositive, remain cubic on cooling rather than going through a symmetry lowering phase transition. $CaTiF_6$ was examined in an effort to expand the range of fluorides known to display strong isotropic NTE over a wide temperature range. The solid state synthesis and an initial characterization of $CaTiF_6$ was reported by Hagenmuller and co-workers in 1970,[39] with subsequent mention by Reinen and Steffen in their 1978 work on structure and bonding in $M^{(II)}M^{(IV)}F_6$.[40]

2. EXPERIMENTAL

2.1. Synthesis

CaF_2 and TiF_4, purchased from Sigma Aldrich and STREM respectively, were ground together in a 1:1 molar ratio under a dry nitrogen atmosphere. The mixture was pressed into a pellet, and placed in a copper tube. The tube was sealed by arc welding in argon, and then sealed inside an evacuated fused quartz ampoule. The ampoule was heated to 400 °C, held at 400 °C for 24 h, annealed at 350 °C for 24 h, and then cooled to room temperature. The reaction produced $CaTiF_6$, as an off-white powder, with ~ 2 wt% CaF_2 as an impurity (see Figure S1).

2.2. High Resolution Variable Temperature X-ray Powder Diffraction Measurements

High resolution x-ray powder diffraction data were collected on the 11-BM beamline at the Advanced Photon Source, Argonne National Laboratory at a wavelength of 0.41272 Å using a sample sealed in a Kapton capillary tube. An Oxford Cryostream 700+ nitrogen gas blower was used for data collection between 300 and 500 K (denoted as "N_2" later in the paper). An Oxford Instruments closed-flow helium cryostat (OptistatCF), denoted "He", was used for data sets between 10 and 300 K.

2.3. High Pressure X-ray Diffraction Measurements

High pressure powder x-ray diffraction data were collected on a Perkin-Elmer amorphous silicon 2D detector, using beamline 17-BM at the Advanced Photon Source, Argonne National Laboratory, at a precisely determined wavelength of 0.45240 Å. These measurements made use of an EasyLab "Diacell Bragg-(G)" diamond anvil cell, which was equipped with a diaphragm so that the pressure could be increased under computer control. A low molecular weight silicone oil (Alfa, MW = 237 g·mol^{-1}) was used as the pressure transmitting medium. Pressure was determined from the lattice constant of CaF_2, which was added as pressure marker, using the equation of state reported by Angel.[41] Data were acquired while the pressure was continuously increased using a syringe pump to supply high pressure methanol to the diaphragm.

2.4. Rietveld Analyses of the Powder Diffraction Data

All Rietveld refinements were performed using the General Structure Analysis System (GSAS) coupled with EXPGUI.[42-43] In the analyses of both the low temperature ambient pressure data and the high pressure ambient temperature data, the fits to the rhombohedral model were less than ideal due to the presence of some scattering between Bragg peak maxima, which is attributed to strain associated with the domain structure that is present once the ferroelastic cubic to rhombohedral transition has occurred.[26] Representative profile fits for the cubic and rhombohedral phases are shown in Figs S1 –S4. As the high pressure data had a high background and relatively low Q_{max} (5.5 Å^{-1}), a structural model consisting of isotropic atomic displacement parameters for each atom and fluorine coordinates was adopted. The accuracy of the structural information from these analyses, especially for pressures close to the phase transition at 3 GPa where there is significant peak broadening, is limited. Parameters for the refined structural models and the lattice constants are reported in the SI.

3. RESULTS AND DISCUSSION

3.1. Response to Heating and Cooling

Above 120 K $CaTiF_6$ adopts a cubic cation ordered ReO_3-type structure. The peak splitting seen in the variable temperature x-ray powder diffraction data suggest a phase transition on cooling to ~ 120 K from cubic ($Fm\bar{3}m$) to rhombohedral ($R\bar{3}$), which involves correlated octahedral tilting (Glazer notation $a^-a^-a^-$).[44] Transitions of this type are commonly seen in ReO_3-type metal fluorides.[45-48]

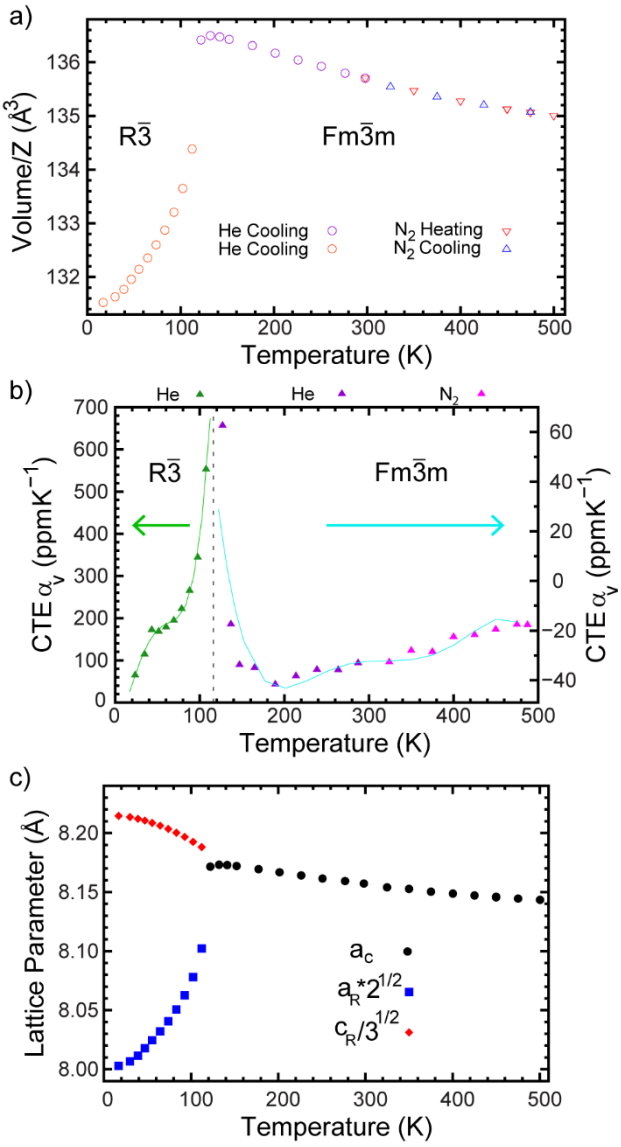

Figure 1: a) Unit cell volume per formula unit, b) volumetric coefficients of thermal expansion (CTE), and c) lattice constant versus temperature for $CaTiF_6$. The curves shown in (b) were obtained by differentiation of six and five term polynomial fits to the unit cell volumes of the cubic and rhombohedral phases, respectively. Additionally, the CTE was determined point by point (purple/magenta and green symbols). He and N_2 denote helium cryostat and nitrogen Cryostream sample environments respectively.

The volume per formula unit, volume thermal expansion coefficients and lattice constants versus temperature obtained from Rietveld analyses are shown in Figure 1. As is typical of ReO_3-type

metal fluorides, the rhombohedral phase shows strong volumetric positive thermal expansion (PTE), which is highly anisotropic.[26, 36] In the rhombohedral phase the octahedra are tilted so the Ti-F-Ca angle is < 180°. As this phase is heated the bond angle increases (~158.8° and ~165.5° at 16 and 112 K respectively), leading to very strong positive thermal expansion in the a-b plane of the hexagonal unit cell. Just above the phase transition temperature the cubic phase displays PTE, which is presumably due to the presence of local structural distortions away from the ideal cubic structure. This interpretation is supported by the atomic displacement (APD) parameters shown in Figure 2; the transverse component of the ADP (U_{22}) for fluorine increases on cooling from 130 to 120 K. Above 130 K the cubic phase of $CaTiF_6$ shows NTE up to the highest temperature studied (500 K). The NTE is strongest at 177 K with a α_v = -42 ppm K^{-1}. The expansion coefficient slowly increases up to -18 ppm K^{-1} at 488 K.

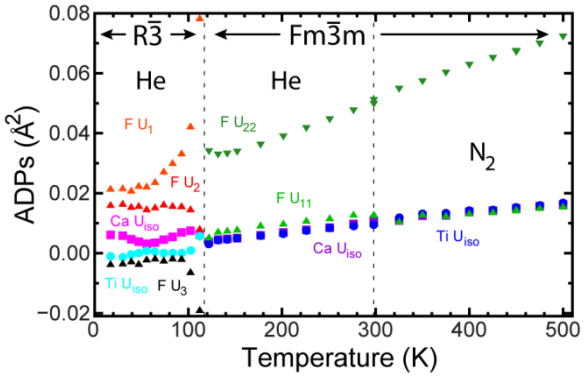

Figure 2: Atomic displacement parameters for $CaTiF_6$ determined by Rietveld analysis of data from variable temperature X-ray diffraction measurements using a helium cryostat (He) and nitrogen Cryostream (N_2). F U_i values are the principle components of the anisotropic atomic displacement ellipsoid for fluorine in the rhombohedral phase.

The thermal expansion of $CaM^{4+}F_6$ (M – Zr, Hf, Nb and Ti) are compared in Figure 3. At low temperatures, the behavior of $CaTiF_6$ is distinct from the other compositions, as it is the only one that undergoes a phase transition on cooling. The ideal cubic form of the ReO_3 structure is reported to be preferred on electrostatic grounds, with the commonly reported distortions away from cubic symmetry perhaps arising from polarization of fluoride or covalency.[49] Titanium has a higher electronegativity (1.32)[50] and smaller size (six coordinate Ti^{4+}, 0.605 Å)[51] than zirconium, hafnium and niobium (1.22, 1.23, 1.23;[50] 0.72 Å, 0.71 Å, 0.68 Å)[51] consistent with the occurrence of a distortion on cooling $CaTiF_6$, but not the other $CaM^{4+}F_6$.

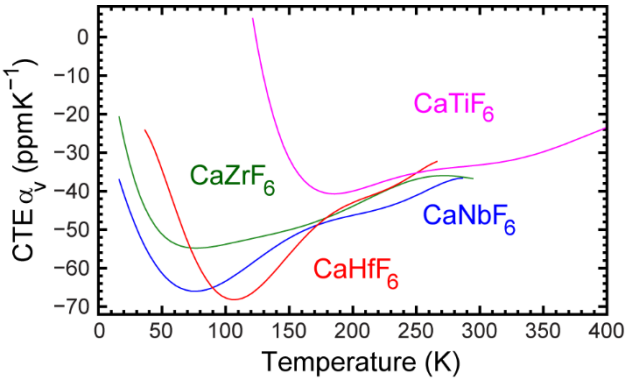

Figure 3: Temperature dependence of the volumetric coefficients of thermal expansion for $CaM^{4+}F_6$ (M – Zr, Hf, Nb, Ti).[26, 28] The curves are six term polynomials, which were fit to the point by point CTE data for each material to best represent the temperature dependence of their thermal expansion.

All four $CaM^{4+}F_6$ have similar CTEs at close to room temperature. However, $CaNbF_6$ and $CaHfF_6$ show the largest NTE at low temperatures, with the volumetric CTE of both dipping down to ~ -70 ppm K^{-1}. The atomic displacement parameters (ADPs) obtained from Rietveld analyses of data for $CaTiF_6$ are shown in Figure 2. The overall pattern for the cubic phase is similar to that previously reported for $CaZrF_6$ and $CaNbF_6$. The transverse component of the ADP for F (U_{22}) is much larger than that of the component parallel to the M-F bonds, strongly dependent on temperature and extrapolates to a large value (~0.02 $Å^2$) at 0 K. This is consistent with a very soft potential for the transverse motion of the fluoride and the NTE in the material being driven by this transverse motion, as is typically the case of cubic ReO_3-type fluorides.[52] Below the phase transition to a rhombohedral structure, the values of the refined atomic displacement parameters are less well behaved. This is likely a consequence of parameter correlations for temperatures just below the transition, where the split peaks associated with the symmetry lowering are poorly resolved, and also less than ideal fits to the data for the rhombohedral material. As mentioned earlier, the poor fits arise because there is scattering between the Bragg presumably due to strains in multiply twinned grains.[26] The refined ADPs for fluorine are consistent with a relatively soft potential for fluorine displacements even in the rhombohedral phase.

3.2. Response to Compression

The high pressure x-ray diffraction data (Figure 4a) recorded at room temperature (~295 K) indicates the occurrence of at least two structural phase transitions in $CaTiF_6$ on compression to 6.5 GPa. Below ~ 0.25 GPa the material is cubic. On increasing pressure, the Bragg peaks split in a fashion consistent with an octahedral tilting transition to a rhombohedral ($R\bar{3}$) phase, as was seen on cooling $CaTiF_6$ to 120 K. Phase coexistence at ~ 0.25 GPa suggests that the transition is first order. Structural transitions of this type commonly occur at low pressures on compressing cubic MF_3 and $MM'F_6$ ReO_3-type phases[26, 53] and they are a potential impediment to application in controlled thermal expansion composites, where the materials are likely to be subject to stresses from thermal expansion mismatch. However, $CaZrF_6$ and $CaNbF_6$ do not display an analogous octahedral tilting transition on compression. Cubic $CaZrF_6$ transforms to a disordered material on compression to ~ 0.4

GPa[28] at room temperature, and cubic $CaNbF_6$ transforms to a new crystalline phase at ~0.4 GPa.[26] These differences may arise in part because both Zr(IV) and Nb(IV) are much larger than Ti(IV), and can more readily accommodate an increase in coordination number.

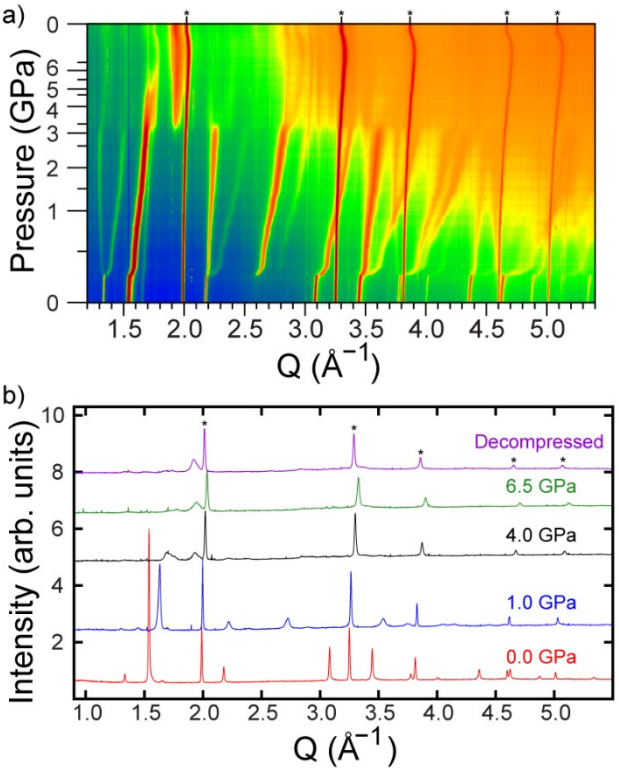

Figure 4: a) x-ray powder diffraction data for $CaTiF_6$ as it is compressed in a diamond anvil cell. b) Diffraction patterns for $CaTiF_6$ at selected pressures. Peaks from the CaF_2 pressure calibrant are marked *.

At ~ 3 GPa a further phase transformation occurs leading to the quite abrupt disappearance of the peak at ~ 2.2 Å^{-1} from the rhombohedral phase and the appearance of broad scattering maxima at ~ 1.75 and 1.9 Å^{-1}. Between 5 and 6 GPa the scattering pattern changes so that is dominated by a single broad maximum at 1.9 Å^{-1}. On decompression, the sample remained essentially amorphous. A comparison of the diffraction patterns in each pressure range of interest is given in Figure 4b.

In Figure 5, unit cell volume versus pressure (P < 0.25 GPa) is shown for cubic $CaTiF_6$ along with a fit to a 3rd order Birch-Murnaghan equation of state, which was performed using EoSFit7.[54] The zero pressure bulk modulus, K_0, was estimated to be ~ 29 GPa, indicating that $CaTiF_6$ is softer than both $CaZrF_6$ and $CaNbF_6$ (K_0 36 and 33.7, respectively). $CaTiF_6$, like several other cubic $MM'F_6$ phases and the anion excess ReO_3-type material $YbZrF_7$,[25] shows strong pressure induced softening, K_0' ~-50(5), prior to undergoing a transformation to a rhombohedral phase. The magnitude of this softening is greater than that seen in both $CaZrF_6$ and $CaNbF_6$ (K_0' of -26 and -23, respectively). Most materials stiffen on compression as volume reduction brings atoms closer together and increases the repulsion between them. However, Dove et al. have argued that framework structures likely to display NTE are also likely to show pressure induced softening.[55-56] Pressure induced softening has previously been reported for the NTE materials ZrW_2O_8 and $Zn(CN)_2$.[57-58]

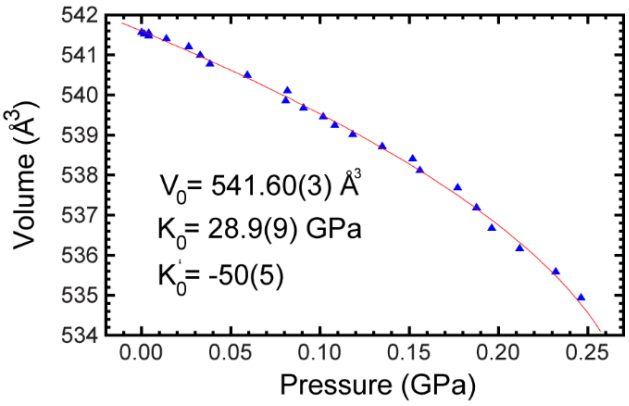

Figure 5: Volume versus pressure for cubic $CaTiF_6$ along with a best fit using a 3rd order Birch-Murnaghan equation of state.

The variation of unit cell volume and lattice constants with pressure (Figure 6) indicates that the elastic properties of rhombohedral ($R\bar{3}$) $CaTiF_6$ are very different from those of the cubic ($Fm\bar{3}m$) phase. In the rhombohedral phase further octahedral tilting ($a^-a^-a^-$), involving rotation around the 3-fold axes of the octahedra, is associated with a reduction in the Ca-F-Ti bond angles (see Figure 7a) and provides a relatively low energy pathway for volume reduction, at least for pressures where the Ca-F-Ti bond angle is significantly above that expected for close packing of the anions.

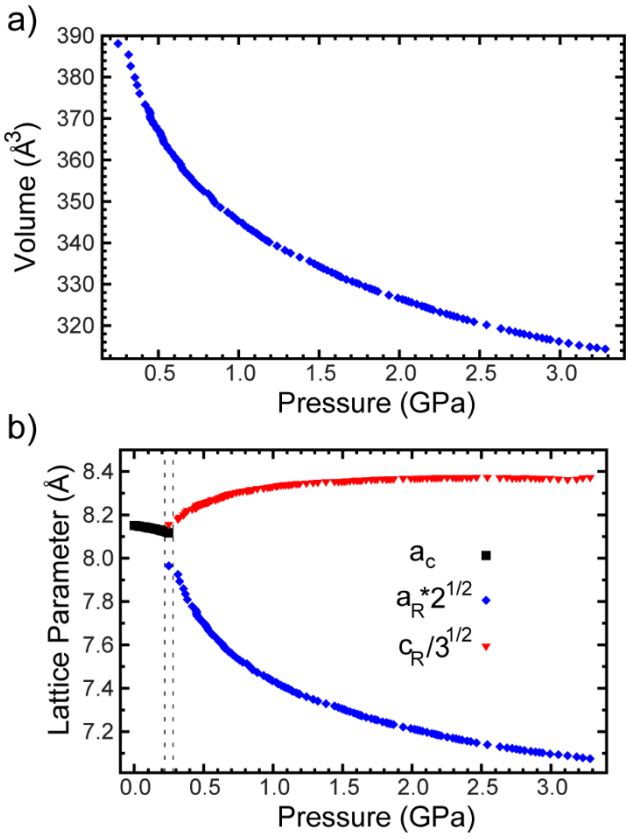

Figure 6: a) Pressure dependence of the unit cell volume, and b) lattice constants for the rhombohedral phase of $CaTiF_6$. The lattice constants for the rhombohedral phase have been scaled so that they can be com-

pared to that of the cubic phase. There is phase coexistence in the region bounded by dashed lines.

The behavior of the rhombohedral phase on compression could not be adequately described using a Birch Murnaghan equation of state. A polynomial fit to ln(V) versus pressure was used to determine how the phase's bulk modulus varied with pressure (Figure S5). At pressures just above the cubic to rhombohedral phase transition the material is very soft, with a bulk modulus of between 3 and 5 GPa for pressures below 0.5 GPa. However, its bulk modulus increases almost linearly on compression, becoming > 30 GPa for pressures higher than 2.5 GPa. This stiffening is presumably due to the structure approaching that where the fluoride is closest packed. The compressibility of the rhombohedral phase is highly anisotropic. In the a-b plane, the material is soft as the volume reducing $a^-a^-a^-$ tilts involve rotation parallel to the c-axis. However, parallel to the crystallographic c-axis the material displays negative linear compressibility (NLC) up to ~2.5 GPa (see Figure 6b). Similar behavior has been reported in rhombohedral FeF_3 and other trifluorides.[59-60] The NLC was attributed to a distortion of the individual octahedra, where the F-F distances between fluorine on an octahedral face lying perpendicular to the c-axis (d_{1M}) decreased more readily on compression than the F-F distances between pairs of fluorine lying on opposite triangular faces of the same octahedron (d_{2M}). This distortion can be quantified as an octahedral strain using $\varepsilon_M = (d_{2M} - d_{1M})/(d_{2M} + d_{1M})$ (see Figure 7b)

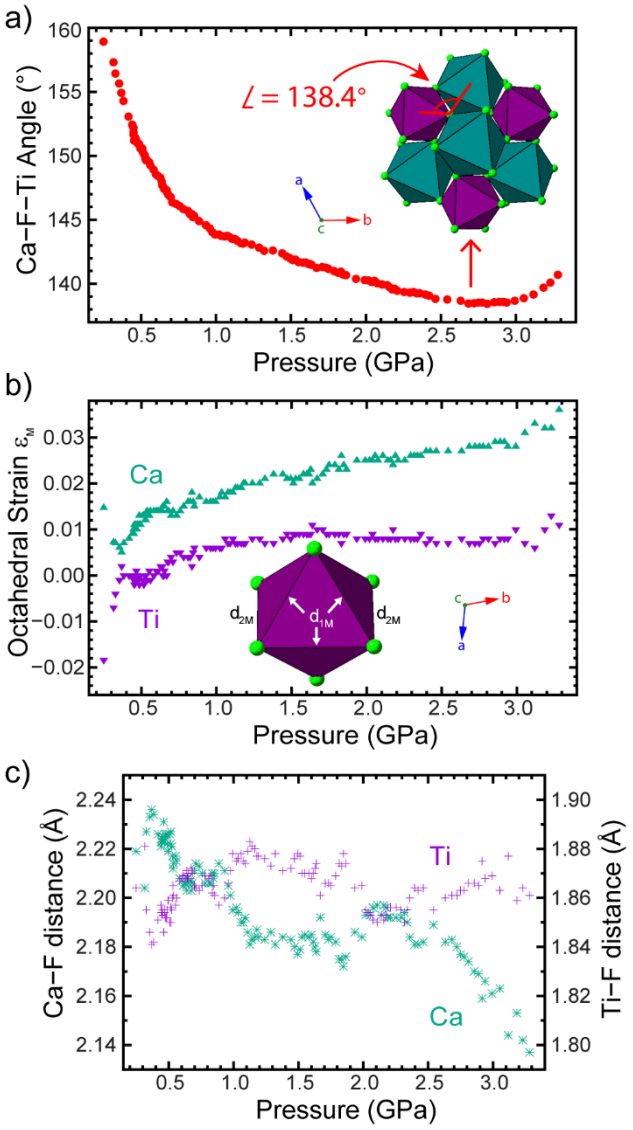

Figure 7: Pressure dependence of a) the Ca-F-Ti bond angle, b) the octahedral strain for the CaF_6 and TiF_6 units, as described in the text, and c) the Ti-F and Ca-F bond lengths.

The CaF_6 and TiF_6 octahedra that make up the rhombohedral structure respond differently to pressure. As might be expected, the longer Ca-F bond lengths are more compressible than the shorter Ti-F distances (Figure 7c), and on compression the CaF_6 units display much greater octahedral strain than the TiF_6 units (Figure 7b). The maximum octahedral strain observed in the TiF_6 units is similar to that reported for FeF_3 on compression, but that seen in the CaF_6 is approximately three times greater.

At ~3 GPa, where rhombohedral $CaTiF_6$ transforms to a poorly ordered material, the Ca-Ti-F bond angle is approaching that expected for close packing (132°), consistent with a phase transition involving a new mechanism for volume reduction on compression.

4. CONCLUSIONS

The behavior of cooling and compressing $CaTiF_6$ is distinct from that of both $CaZrF_6$ and $CaNbF_6$, but similar to that of $MgZrF_6$.[26, 28] $CaTiF_6$ undergoes an octahedral tilting transition on cooling below 120 K, which leads to anisotropic positive volume thermal expan-

sion at low temperature, whereas $CaZrF_6$ and $CaNbF_6$ remain cubic to at least 10 K. This difference may be associated with the smaller size and higher electronegativity of Ti^{4+}, as highly ionic bonding is thought to favor the cubic structure over distorted variants. $CaTiF_6$ also undergoes an octahedral tilting transition on compression at ambient temperature. This is in contrast to $CaZrF_6$ and $CaNbF_6$, where other volume reduction mechanisms lead at ~ 0.4 GPa to disordering in the case of $CaZrF_6$ and what appears to be a reconstructive crystal to crystal transition in $CaNbF_6$. The pressure induced cubic to rhombohedral transition in $CaTiF_6$ at 0.25 GPa is likely to limit its potential for application in controlled thermal expansion composites, as in such a composite it would experience stresses due to thermal expansion mismatch.

ASSOCIATED CONTENT

Supporting Information. Example Rietveld fits, octahedral distortion on compression, structural information, bulk modulus versus pressure, lattice constants versus temperature and pressure. This material is available free of charge via the Internet at http://pubs.acs.org.

AUTHOR INFORMATION

Corresponding Author

* E-mail: angus.wilkinson@chemistry.gatech.edu

ORCID

Angus P. Wilkinson: 0000-0003-2904-400X

Notes

The authors declare no competing financial interest.

ACKNOWLEDGEMENT

We are grateful to Anthony Lloyd, Sam Baxter, Ross Angel and Saul Lapidus for assistance with various aspects of the experiments and data analysis. The activities at Georgia Tech were supported in part under NSF DMR-1607316. This work made use of the Advanced Photon Source, a U.S. Department of Energy (DOE) Office of Science User Facility operated for the DOE Office of Science by Argonne National Laboratory under contract DE-AC02-06CH11357.

REFERENCES

1. Badrinarayanan, P.; Kessler, M. R., Zirconium Tungstate/Cyanate Ester Nanocomposites with Tailored Thermal Expansivity. *Compos. Sci. Technol.* **2011,** *71*, 1385-1391.

2. Balch, D. K.; Dunand, D. C., Copper-Zirconium Tungstate Composites Exhibiting Low and Negative Thermal Expansion Influenced by Reinforcement Phase Transformations. *Metall. Mater. Trans. A* **2004,** *35A*, 1159-1165.

3. Chandra, A.; Meyer, W. H.; Best, A.; Hanewald, A.; Wegner, G., Modifying Thermal Expansion of Polymer Composites by Blending with a Negative Thermal Expansion Material. *Macromol. Mater. Eng.* **2007,** *292*, 295-301.

4. Della Gaspera, E.; Tucker, R.; Star, K.; Lan, E. H.; Ju, Y. S.; Dunn, B., Copper-Based Conductive Composites with Tailored Thermal Expansion. *ACS Appl. Mater. Interfaces* **2013,** *5*, 10966-74.

5. Holzer, H.; Dunand, D. C., Phase transformation and thermal expansion of Cu/ZrW_2O_8 metal matrix composites. *J. Mater. Res.* **1999,** *14*, 780-789.

6. Lind, C.; Coleman, M. R.; Kozy, L. C.; Sharma, G. R., Zirconium Tungstate/Polymer Nanocomposites: Challenges and Opportunities. *Phys. Status Solidi B* **2011,** *248*, 123-129.

7. Mavoori, H.; Jin, S., Low-Thermal-Expansion Copper Composites via Negative CTE Metallic Elements. *J. Metals* **1998**, 70-72.

8. Sigmund, O.; Torquato, S., Composites with Extremal Thermal Expansion Coefficients. *Appl. Phys. Lett.* **1996,** *69*, 3203-3205.

9. Takenaka, K., Negative Thermal Expansion Materials: Technological Key for Control of Thermal Expansion. *Sci. Technol. Adv. Mater.* **2012,** *13*.

10. Morelock, C. R.; Suchomel, M. R.; Wilkinson, A. P., A Cautionary Tale on the Use of GE-7031 Varnish: Low Temperature Thermal Expansion Studies of ScF_3. *J. Appl. Crystallogr.* **2013,** *46*, 823-825.

11. Miller, W.; Smith, C. W.; Dooling, P.; Burgess, A. N.; Evans, K. E., Reduced Thermal Stress in Composites via Negative Thermal Expansion Particulate Fillers. *Compos. Sci. Technol.* **2010,** *70*, 318-327.

12. Yilmaz, S.; Dunand, D. C., Finite-element analysis of thermal expansion and thermal mismatch stresses in a Cu 60vol% ZrW_2O_8 composite. *Compos. Sci. Technol.* **2004,** *64*, 1895-1898.

13. Chen, J.; Hu, L.; Deng, J.; Xing, X., Negative thermal expansion in functional materials: controllable thermal expansion by chemical modifications. *Chem. Soc. Rev.* **2015,** *44*, 3522-3567.

14. Lind, C., Two Decades of Negative Thermal Expansion Research: Where Do We Stand? *Materials* **2012,** *5*, 1125-1154.

15. Azuma, M.; Chen, W.-t.; Seki, H.; Czapski, M.; Olga, S.; Oka, K.; Mizumaki, M.; Watanuki, T.; Ishimatsu, N.; Kawamura, N.; Ishiwata, S.; Tucker, M. G.; Shimakawa, Y.; Attfield, J. P., Colossal Negative Thermal Expansion in $BiNiO_3$ Induced by Intermetallic Charge Transfer. *Nat. Commun.* **2011,** *2*.

16. Ikuya, Y.; Kazuki, T.; Kenya, O.; Naoaki, H.; Jungeun, K.; Naruki, T.; Ryoji, T.; Masafumi, M.; Norimasa, N.; Toru, I.; Tetsuo, I.; Kenichi, K.; Masaki, T.; Mikio, T., Giant Negative Thermal Expansion in the Iron Perovskite $SrCu_3Fe_4O_{12}$. *Angew. Chem. Int. Ed. Engl.* **2011,** *50*, 6579-6582.

17. Takenaka, K.; Takagi, H., Giant Negative Thermal Expansion in Ge-Doped Anti-perovskite Manganese Nitrides. *Appl. Phys. Lett.* **2005,** *87*, 261902:(3).

18. Zhao, Y.-Y.; Hu, F.-X.; Bao, L.-F.; Wang, J.; Wu, H.; Huang, Q.-Z.; Wu, R.-R.; Liu, Y.; Shen, F.-R.; Kuang, H.; Zhang, M.; Zuo, W.-L.; Zheng, X.-Q.; Sun, J.-R.; Shen, B.-G., Giant Negative Thermal Expansion in Bonded MnCoGe-Based Compounds with Ni_2In-type Hexagonal Structure. *J. Am. Chem. Soc.* **2015,** *137*, 1746-1749.

19. Evans, J. S. O.; Mary, T. A.; Vogt, T.; Subramanian, M. A.; Sleight, A. W., Negative Thermal Expansion in ZrW_2O_8 and HfW_2O_8. *Chem. Mater.* **1996,** *8*, 2809-2823.

20. Wu, Y.; Kobayashi, A.; Halder, G. J.; Peterson, V. K.; Chapman, K. W.; Lock, N.; Southon, P. D.; Kepert, C. J., Negative Thermal Expansion in the Metal–Organic Framework Material Cu_3(1,3,5-benzenetricarboxylate)$_2$. *Angew. Chem. Int. Ed. Engl.* **2008,** *120*, 9061-9064.

21. Goodwin, A. L.; Kepert, C. J., Negative Thermal Expansion and Low-Frequency Modes in Cyanide-Bridged Framework Materials. *Phys. Rev. B* **2005,** *71*, 140301:(4).

22. Greve, B. K.; Martin, K. L.; Lee, P. L.; Chupas, P. J.; Chapman, K. W.; Wilkinson, A. P., Pronounced Negative Thermal Expansion from a Simple Structure: Cubic ScF_3. *J. Am. Chem. Soc.* **2010,** *132*, 15496-15498.

23. Evans, J. S. O.; Hu, Z.; Jorgensen, J. D.; Argyriou, D. N.; Short, S.; Sleight, A. W., Compressibility, Phase Transitions, and Oxygen Migration in Zirconium Tungstate, ZrW_2O_8. *Science* **1997,** *275*, 61-65.

24. Chapman, K. W.; Halder, G. J.; Chupas, P. J., Pressure-Induced Amorphization and Porosity Modification in a Metal−Organic Framework. *J. Am. Chem. Soc.* **2009,** *131*, 17546-17547.

25. Ticknor, J. O.; Hester, B. R.; Adkins, J. W.; Xu, W.; Yakovenko, A. A.; Wilkinson, A. P., Zero Thermal Expansion and Abrupt Amorphization on Compression in Anion Excess ReO_3-type Cubic $YbZrF_7$. *Chem. Mater.* **2018.**

26. Hester, B. R.; Hancock, J. C.; Lapidus, S. H.; Wilkinson, A. P., Composition, Response to Pressure, and Negative Thermal Expansion in $M^{II}B^{IV}F_6$ (M = Ca, Mg; B = Zr, Nb). *Chem. Mater.* **2017,** *29*, 823-831.

27. Morelock, C. R.; Gallington, L. C.; Wilkinson, A. P., Solid Solubility, Phase Transitions, Thermal Expansion, and Compressibility in $Sc_{1-x}Al_xF_3$. *J. Solid State Chem.* **2015,** *222,* 96-102.

28. Hancock, J. C.; Chapman, K. W.; Halder, G. J.; Morelock, C. R.; Kaplan, B. S.; Gallington, L. C.; Bongiorno, A.; Han, C.; Zhou, S.; Wilkinson, A. P., Large Negative Thermal Expansion and Anomalous Behavior on Compression in Cubic ReO_3-type $A^{II}B^{IV}F_6$: $CaZrF_6$ and $CaHfF_6$. *Chem. Mater.* **2015**.

29. Morelock, C. R.; Gallington, L. C.; Wilkinson, A. P., Evolution of Negative Thermal Expansion and Phase Transitions in $Sc_{1-x}Ti_xF_3$. *Chem. Mater.* **2014,** *26,* 1936-1940.

30. Morelock, C. R.; Greve, B. K.; Gallington, L. C.; Chapman, K. W.; Wilkinson, A. P., Negative Thermal Expansion and Compressibility of $Sc_{1-x}Y_xF_3$ ($x < 0.25$). *J. Appl. Phys.* **2013,** *114,* 213501.

31. Yang, C.; Zhang, Y.; Bai, J.; Qu, B.; Tong, P.; Wang, M.; Lin, J.; Zhang, R.; Tong, H.; Wu, Y.; Song, W.; Sun, Y., Crossover of Thermal Expansion from Positive to Negative by Removing the Excess Fluorines in Cubic ReO_3-type $TiZrF_{7-x}$. *J. Mater. Chem.* **2018**.

32. Qin, F.; Chen, J.; Aydemir, U.; Sanson, A.; Wang, L.; Pan, Z.; Xu, J.; Sun, C.; Ren, Y.; Deng, J.; Yu, R.; Hu, L.; Snyder, G. J.; Xing, X., Isotropic Zero Thermal Expansion and Local Vibrational Dynamics in $(Sc,Fe)F_3$. *Inorg. Chem.* **2017,** *56,* 10840-10843.

33. Han, F.; Hu, L.; Liu, Z.; Li, Q.; Wang, T.; Ren, Y.; Deng, J.; Chen, J.; Xing, X., Local Structure and Controllable Thermal Expansion in the Solid Solution $(Mn_{1-x}Ni_x)ZrF_6$. *Inorg. Chem. Front.* **2017**.

34. Chen, J.; Gao, Q.; Sanson, A.; Jiang, X.; Huang, Q.; Carnera, A.; Rodriguez, C. G.; Olivi, L.; Wang, L.; Hu, L.; Lin, K.; Ren, Y.; Lin, Z.; Wang, C.; Gu, L.; Deng, J.; Attfield, J. P.; Xing, X., Tunable Thermal Expansion in Framework Materials through Redox Intercalation. *Nat. Commun.* **2017,** *8,* 14441.

35. Wang, T.; Xu, J.; Hu, L.; Wang, W.; Huang, R.; Han, F.; Pan, Z.; Deng, J.; Ren, Y.; Li, L.; Chen, J.; Xing, X., Tunable Thermal Expansion and Magnetism in Zr-Doped ScF_3. *Appl. Phys. Lett.* **2016,** *109,* 181901.

36. Hu, L.; Chen, J.; Xu, J.; Wang, N.; Han, F.; Ren, Y.; Pan, Z.; Rong, Y.; Huang, R.; Deng, J.; Li, L.; Xing, X., Atomic Linkage Flexibility Tuned Isotropic Negative, Zero, and Positive Thermal Expansion in $MZrF_6$ (M = Ca, Mn, Fe, Co, Ni, and Zn). *J. Am. Chem. Soc.* **2016,** *138,* 14530-14533.

37. Hu, L.; Chen, J.; Fan, L.; Ren, Y.; Huang, Q.; Sanson, A.; Jiang, Z.; Zhou, M.; Rong, Y.; Wang, Y.; Deng, J.; Xing, X., High-Curie-Temperature Ferromagnetism in $(Sc,Fe)F_3$ Fluorides and its Dependence on Chemical Valence. *Adv. Mater.* **2015,** *27,* 4592-4596.

38. Hu, L.; Chen, J.; Fan, L.; Ren, Y.; Rong, Y.; Pan, Z.; Deng, J.; Yu, R.; Xing, X., Zero Thermal Expansion and Ferromagnetism in Cubic $Sc_{1-x}M_xF_3$ (M = Ga, Fe) over a Wide Temperature Range. *J. Am. Chem. Soc.* **2014,** *136,* 13566-13569.

39. Ravez, J.; Vassilia.M; Muhll, R. V. D.; Hagenmuller, P., Les systems MF_2-TIF_4 (M=Ca, Sr, Ba)). *Revue de Chimie minerale* **1970,** *7,* 967-973.

40. Reinen, D.; Steffens, F., Structure and Bonding in Transition-Metal Fluorides $M^{II}Me^{IV}F_6$ .A. Phase-Transitions. *Z. Anorg. Allg. Chem.* **1978,** *441,* 63-82.

41. Angel, R. J., The High-Pressure, High Temperature Equation of State of Calcium Fluoride, CaF_2. *J. Phys. Condens. Matter* **1993,** *5,* L141-L144.

42. Larson, A. C.; Von Dreele, R. B., *GSAS - General Structure Analysis System*. Report LA-UR-86-748: Los Alamos Laboratory, 1987.

43. Toby, B. H., EXPGUI, a Graphical User Interface for GSAS. *J. Appl. Crystallogr.* **2001,** *34,* 210-213.

44. Glazer, A. M., Classification of Tilted Octahedra in Perovskites. *Acta Crystallogr.* **1972,** *B28,* 3384-3392.

45. Blank, H. R.; Frank, M.; Geiger, M.; Greneche, J. M.; Ismaier, M.; Kaltenhauser, M.; Kapp, R.; Kreische, W.; Leblanc, M.; Lossen, U.; Zapf, B., Systematic Investigations of MF_3 Crystalline Compounds (M = Al, Cr, Fe, Ga, In, Sc, Ti, and V) and $Fe_{1-X}M_XF_3$ Mixed Series (M = Ga, Cr, V). *Z.Naturforsch.(A)* **1994,** *49,* 361-366.

46. Daniel, P.; Bulou, A.; Rousseau, M.; Nouet, J., Structural Phase-Transitions and Lattice-Dynamics in the Trifluorides MF_3 (M = Al, Cr, Ga, V, Fe, In ...). *Phase Transitions* **1991,** *33,* 91-97.

47. Kennedy, B. J.; Vogt, T., Powder X-ray Diffraction Study of the Rhombohedral to Cubic Phase Transition in TiF_3. *Mater. Res. Bull.* **2002,** *37,* 77-83.

48. Mogusmilankovic, A.; Ravez, J.; Chaminade, J. P.; Hagenmuller, P., Ferroelastic Properties of TiF_3, VF_3, CrF_3, FeF_3, GaF_3, Compounds. *Mater. Res. Bull.* **1985,** *20,* 9-17.

49. Herzig, P.; Zemann, J., AB_3 Nets Built from Corner-Connected Octahedra - Geometries, Electrosctatic Lattice Energies, and Stereochemical Discussion. *Z. Krist.* **1993,** *205,* 85-97.

50. Little, E. J.; Jones, M. M., A Complete Table of Electronegativities. *J. Chem. Ed.* **1960,** *37,* 231.

51. Shannon, R., Revised Effective Ionic Radii and Systematic Studies of Interatomic Distances in Halides and Chalcogenides. *Acta Crystallogr. Sect. A* **1976,** *32,* 751-767.

52. Hu, L.; Chen, J.; Sanson, A.; Wu, H.; Guglieri Rodriguez, C.; Olivi, L.; Ren, Y.; Fan, L.; Deng, J.; Xing, X., New Insights into the Negative Thermal Expansion: Direct Experimental Evidence for the "Guitar-String" Effect in Cubic ScF_3. *J. Am. Chem. Soc.* **2016,** *138,* 8320-8323.

53. Aleksandrov, K. S.; Voronov, V. N.; Vtyurin, A. N.; Goryainov, S. V.; Zamkova, N. G.; Zinenko, V. I.; Krylov, A. S., Lattice Dynamics and Hydrostatic-Pressure-Induced Phase Transitions in ScF_3. *J. Exp. Theor. Phys.* **2002,** *94,* 977-984.

54. Angel, R. J.; Gonzalez-Platas, J.; Alvaro, M., EosFit7c and a Fortran Module (Library) for Equation of State Calculations. *Z. Krist.* **2014,** *229,* 405-419.

55. Fang, H.; Dove, M. T., Pressure-Induced Softening as a Common Feature of Framework Structures with Negative Thermal Expansion. *Phys. Rev. B* **2013,** *87,* 214109.

56. Hong, F.; Martin, T. D., A Phenomenological Expression to Describe the Temperature Dependence of Pressure-Induced Softening in Negative Thermal Expansion Materials. *J. Phys. Condens. Matter* **2014,** *26,* 115402.

57. Pantea, C.; Migliori, A.; Littlewood, P. B.; Zhao, Y.; Ledbetter, H.; Lashley, J. C.; Kimura, T.; Van Duijn, J.; Kowach, G. R., Pressure-Induced Elastic Softening of Monocrystalline Zirconium Tungstate at 300 K. *Phys. Rev. B* **2006,** *73,* 214118.

58. Fang, H.; Phillips, A. E.; Dove, M. T.; Tucker, M. G.; Goodwin, A. L., Temperature-Dependent Pressure-Induced Softening in $Zn(CN)_2$. *Phys. Rev. B* **2013,** *88,* 144103.

59. Jorgensen, J. E.; Marshall, W. G.; Smith, R. I., The Compression Mechanism of CrF_3. *Acta Crystallogr. Sect. B* **2004,** *60,* 669-673.

60. Jorgensen, J. E.; Smith, R. I., On the Compression Mechanism of FeF_3. *Acta Crystallogr. Sect. B* **2006,** *62,* 987-992.

For Table of Contents Only

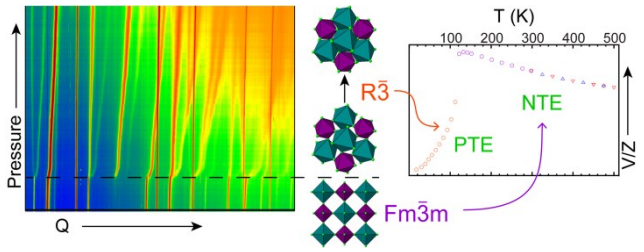

Synopsis

$CaTiF_6$ was examined in an effort to expand the small family of fluorides known to retain the cubic ReO_3-type structure to low temperature and display very strong negative thermal expansion. However, it undergoes a cubic ($Fm\bar{3}m$) to rhombohedral ($R\bar{3}$) transition on cooling to 120 K. On compression it shows very strong pressure induced softening and only remains cubic to ~0.25 GPa. Immediately above this pressure, the material is elastically very soft and displays negative linear compressibility.